Journal of Power Sources 186 (2009) 178–184

Contents lists available at ScienceDirect

Journal of Power Sources

journal homepage: www.elsevier.com/locate/jpowsour

Hydrogen production by steam reforming of liquefied natural gas (LNG) over nickel catalysts supported on cationic surfactant-templated mesoporous aluminas

Jeong Gil Seo[a], Min Hye Youn[a], Sunyoung Park[a], Ji Chul Jung[a], Pil Kim[b], Jin Suk Chung[c], In Kyu Song[a,*]

[a] School of Chemical and Biological Engineering, Research Center for Energy Conversion and Storage, Seoul National University, Shinlim-dong, Kwanak-ku, Seoul 151-744, South Korea
[b] School of Environmental and Chemical Engineering, Chonbuk National University, Chonbuk 561-756, South Korea
[c] School of Chemical Engineering and Bioengineering, University of Ulsan, Ulsan 680-749, South Korea

ARTICLE INFO

Article history:
Received 5 May 2008
Received in revised form 18 August 2008
Accepted 8 September 2008
Available online 27 September 2008

Keywords:
Mesoporous alumina
Nickel catalyst
Liquefied natural gas
Steam reforming
Hydrogen production
Fuel cell

ABSTRACT

Two types of mesoporous γ-aluminas (denoted as A-A and A-S) are prepared by a hydrothermal method under different basic conditions using cationic surfactant (cetyltrimethylammonium bromide, CTAB) as a templating agent. A-A and A-S are synthesized in a medium of ammonia solution and sodium hydroxide solution, respectively. Ni/γ-Al_2O_3 catalysts (Ni/A-A and Ni/A-S) are then prepared by an impregnation method, and are applied to hydrogen production by steam reforming of liquefied natural gas (LNG). The effect of a mesoporous γ-Al_2O_3 support on the catalytic performance of Ni/γ-Al_2O_3 is investigated. The identity of basic solution strongly affects the physical properties of the A-A and A-S supports. The high surface-area of the mesoporous γ-aluminas and the strong metal–support interaction of supported catalysts greatly enhance the dispersion of nickel species on the catalyst surface. The well-developed mesopores of the Ni/A-A and Ni/A-S catalysts prohibit the polymerization of carbon species on the catalyst surface during the reaction. In the steam reforming of LNG, both Ni/A-A and Ni/A-S catalysts give better catalytic performance than the nickel catalyst supported on commercial γ-Al_2O_3 (Ni/A-C). In addition, the Ni/A-A catalyst is superior to the Ni/A-S catalyst. The relatively strong metal–support interaction of Ni/A-A catalyst effectively suppresses the sintering of metallic nickel and the carbon deposition in the steam reforming of LNG. The large pores of the Ni/A-A catalyst also play an important role in enhancing internal mass transfer during the reaction.

1. Introduction

Steam reforming of methane has been widely investigated for the production of hydrogen [1–4]. In particular, low-temperature steam reforming technology has attracted much attention, because of its potential applicability in fuel cell systems. Liquefied natural gas (LNG), which is abundant and mainly composed of methane, can serve as a promising source for hydrogen production by steam reforming. LNG pipelines may become more widespread in the future, which will make LNG well suited as a hydrogen source for residential reformers in fuel cell applications.

Ni/α-Al_2O_3 have been utilized as conventional and economical catalysts for hydrogen production by steam reforming of methane due to their low cost and high intrinsic catalytic activity [5–8]. Nevertheless, the dispersion of nickel species in the Ni/α-Al_2O_3 catalyst is so poor that the maximum allowable nickel loading on the α-Al_2O_3 support does not exceed 12 wt% [9]. Therefore, the Ni/α-Al_2O_3 catalyst has not been readily employed for low-temperature reforming reactions as these require a finely-dispersed nickel catalyst.

High loaded and finely-dispersed nickel catalyst can be obtained by employing transition aluminas, such as γ-, δ-, and θ-Al_2O_3, as supports due to their superior physical and chemical properties compared with α-Al_2O_3. Among various transition aluminas, γ-Al_2O_3 which retains high surface-area and excellent acid-base properties has been widely employed as a catalyst support in many reactions [10-12]. Several problems still remain to be solved in the application of γ-Al_2O_3 as a support for the nickel catalyst required in low-temperature steam reforming reactions. For example, carbon deposition causing a severe catalyst deactivation is accelerated

* Corresponding author. Tel.: +82 2 880 9227; fax: +82 2 889 7415.
E-mail address: inksong@snu.ac.kr (I.K. Song).

0378-7753/$ – see front matter © 2008 Elsevier B.V. All rights reserved.
doi:10.1016/j.jpowsour.2008.09.071

by the strong surface acid sites of γ-Al_2O_3. Sintering of nickel particles can also be induced by the phase transformation of γ-Al_2O_3 to α-Al_2O_3, resulting in loss of active sites of the catalyst. Therefore, many attempts have been made to increase the stability of Ni/γ-Al_2O_3 catalyst in the steam reforming reactions. It has been reported [6,13–15] that the addition of small amount of barrier or thermal stabilizer enhances the steam reforming performance of Ni/γ-Al_2O_3 catalyst. The modification of the supporting material can also be a promising approach to achieving high catalytic performance from the Ni/γ-Al_2O_3 catalyst. For example, it is known that a mesoporous alumina support greatly enhances the coking resistance of nickel-based catalysts, resulting in high performance in the reforming reactions [16,17].

Mesoporous γ-Al_2O_3 can be synthesized by a templating method using anionic [18], cationic [19,20] and non-ionic [21] surfactants. Among these surfactant materials, cationic surfactants have been widely used for the synthesis of mesoporous aluminas. To the best of our knowledge, however, surfactant-templated mesoporous γ-Al_2O_3 has never been used as a support for a nickel catalyst in the reforming reaction. Therefore, the development of cationic surfactant-templated mesoporous γ-Al_2O_3 supports for the nickel catalyst in hydrogen production by steam reforming of LNG is of great interest.

In this work, mesoporous γ-aluminas are prepared by a hydrothermal method under different basic conditions using cationic surfactant (cetyltrimethylammonium bromide, CTAB) as a templating agent for use as supports for nickel catalysts. Ni/γ-Al_2O_3 catalysts are then prepared by an impregnation method, and are applied to hydrogen production by steam reforming of LNG. The effect of a mesoporous γ-Al_2O_3 support on the reforming performance of Ni/γ-Al_2O_3 is examined.

2. Experimental

2.1. Preparation of γ-Al_2O_3 supports and Ni/γ-Al_2O_3 catalysts

γ-Al_2O_3 supports were prepared by a hydrothermal method, according to similar methods reported in the literatures [19,20,22]. Fig. 1 shows the schematic procedure for the preparation of γ-Al_2O_3 by a hydrothermal method using a cationic surfactant as a templating agent. 9 g of cationic surfactant (cetyltrimethylammonium bromide, CTAB, Sigma–Aldrich) was dissolved in 90 ml of deionized water at 80 °C under vigorous stirring. The surfactant solution was maintained for a few minutes to obtain a clear micelle solution. Either 10 ml of ammonia solution or 10 ml of sodium hydroxide solution was then added to the resulting solution to obtain a basic micelle solution (pH 12.5). 13 g of aluminum precursor (aluminum *sec*-butoxide, Sigma–Aldrich) was separately added to 12 ml of hydrolysis retarding agent (2,4-pentanedione, Sigma–Aldrich) to obtain a clear solution of the chelated aluminum precursor. The prepared aluminum precursor solution was slowly added to the basic micelle solution under constant stirring, until a white precipitate was formed. After maintaining the precipitate solution at 80 °C for 5 h, it was hydrothermally treated at 100 °C for 3 days for complete hydrolysis and condensation of the aluminum precursor. The resulting gel was aged for 2 days, and then dried overnight at 120 °C. The resulting powder was finally calcined at 700 °C for 5 h with an air stream to yield a mesoporous γ-Al_2O_3 support. The γ-Al_2O_3 supports prepared in a medium of ammonia solution and sodium hydroxide solution were denoted as A-A and A-S, respectively.

Nickel catalysts supported on mesoporous γ-Al_2O_3 supports (A-A and A-S) were prepared by impregnating a known amount of nickel precursor ($Ni(NO_3)_2{\cdot}6H_2O$, Sigma–Aldrich) on A-A and A-S supports. The prepared Ni/γ-Al_2O_3 catalysts were denoted as Ni/A-A and Ni/A-S. For the purpose of comparison, a nickel catalyst supported on commercial γ-Al_2O_3 (Degussa, denoted as A-C) was also prepared by an impregnation method. The nickel catalyst supported on commercial γ-Al_2O_3 was denoted as Ni/A-C. The nickel loading was fixed at 20 wt% in all cases.

2.2. Characterization

Nitrogen adsorption–desorption isotherms were obtained with an ASAP-2010 (Micromeritics) instrument, and pore-size distributions were determined by the Barret–Joyner–Hallender (BJH) method applied to the desorption branch of the nitrogen isotherm. Crystalline phases of the supports and supported catalysts were investigated by X-ray diffraction (XRD) (MAC Science, M18XHF-SRA) measurements using Cu-Kα radiation (λ = 1.54056 Å) operated at 50 kV and 100 mA. In order to examine the reducibility of supported Ni catalysts, temperature-programmed reduction (TPR) measurements were carried out in a conventional flow system with a moisture trap connected to a thermal conductivity detector (TCD) at temperatures ranging from room temperature to 1000 °C with a

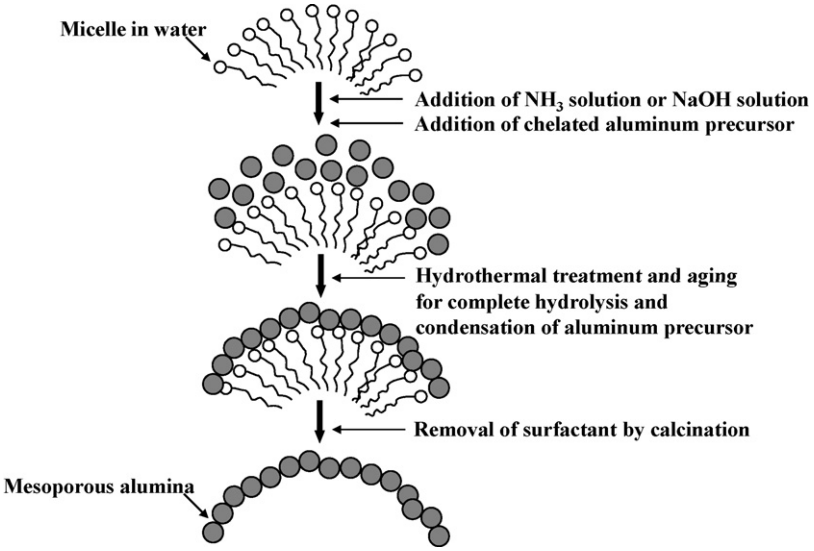

Fig. 1. Schematic procedure for preparation of γ-Al_2O_3 support by a hydrothermal method using cationic surfactant as a templating agent.

ramping rate of 5 °C min^{-1}. For TPR measurements, a mixed stream of H_2 (2 ml min^{-1}) and N_2 (20 ml min^{-1}) was used for 0.2 g of catalyst sample. Transmission electron microscopy (TEM) analyses (Jeol, JEM-2000EXII) were conducted to examine the morphology of supports and to observe carbon deposition on the used catalysts.

2.3. Steam reforming of LNG

Steam reforming of LNG was carried out in a continuous flow fixed-bed reactor at atmospheric pressure. Each calcined catalyst (100 mg) was charged into a tubular quartz reactor, and it was then reduced with a mixed stream of H_2 (3 ml min^{-1}) and N_2 (30 ml min^{-1}) at 700 °C for 3 h. Water was sufficiently vapourized by passing through a pre-heating zone and continuously fed into the reactor together with LNG (92.0 vol.% CH_4 and 8.0 vol.% C_2H_6, LNG flow rate = 5 ml min^{-1}) and a N_2 carrier (30 ml min^{-1}). The steam:carbon ratio in the feed stream was fixed at 2.0, and the total feed rate with respect to the catalyst was maintained at 27 000 ml h^{-1} g^{-1}. The catalytic reaction was carried out at 600 °C. The reaction products were periodically sampled and analyzed using an on-line gas chromatograph (Younglin, ACME 6000) equipped with a thermal conductivity detector (TCD). LNG conversion and hydrogen composition in dry gas were calculated according to the following equations on the basis of carbon balance.

$$LNG\ conversion\,(\%) = \left(1 - \frac{F_{CH_4,out} + F_{C_2H_6,out}}{F_{CH_4,in} + F_{C_2H_6,in}}\right) \times 100 \quad (1)$$

$$H_2\ composition\ in\ dry\ gas\,(\%) = \frac{F_{H_2,out}}{F_{H_2,out} + F_{CH_4,out} + F_{C_2H_6,out} + F_{CO,out} + F_{CO_2,out}} \times 100 \quad (2)$$

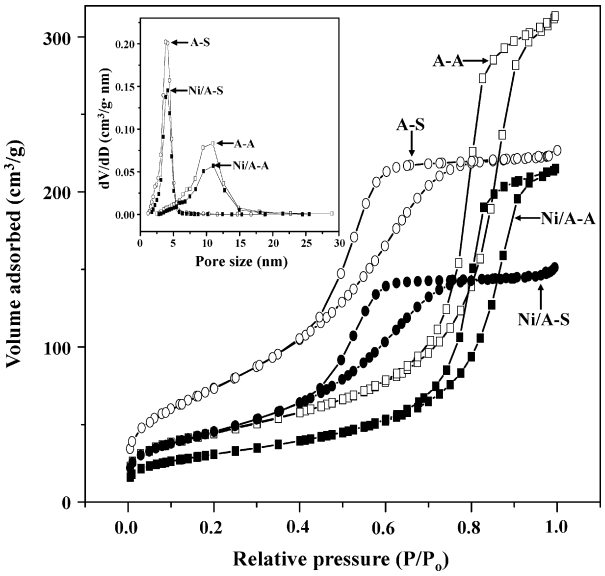

Fig. 2. Nitrogen adsorption–desorption isotherms and pore-size distributions (inset) of supports (A-A and A-S) and supported catalysts (Ni/A-A and Ni/A-S). Supports and supported catalysts calcined at 700 °C prior to the measurements.

3. Results and discussion

3.1. Physical property of supports and supported catalysts

The physical properties of supports and supported catalysts were examined by nitrogen adsorption–desorption isotherm measurements. Fig. 2 shows the nitrogen adsorption–desorption isotherms and BJH pore-size distributions (inset) of supports (A-A and A-S) and supported catalysts (Ni/A-A and Ni/A-S). It is interesting to note that the identity of basic solution strongly affected the

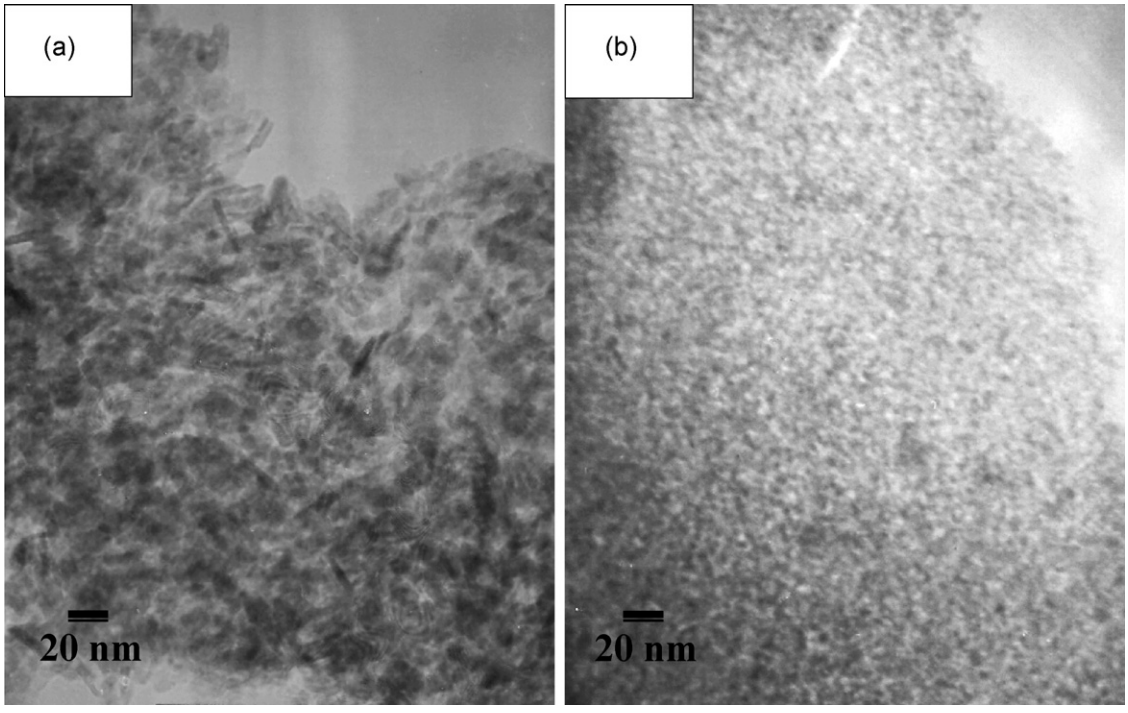

Fig. 3. TEM images of (a) A-A and (b) A-S supports calcined at 700 °C.

physical properties of supports and supported catalysts. A-S and Ni/A-S samples clearly show typical IV-type isotherms with H2-type hysteresis loops, indicating the existence of a well-developed framework mesopore with a narrow pore-size distribution. The desorption branch of A-A and Ni/A-A samples occurs at higher relative pressures ($P/P_o = 0.6$) than that of A-S and Ni/A-S samples ($P/P_o = 0.4$). This suggests the existence of textural mesopores with a broad pore-size distribution in the A-A and Ni/A-A samples [23,24]. These results are further confirmed by BJH pore-size distributions. A-S and Ni/A-S samples exhibit narrow pore-size distributions centred at 3.5 and 3.7 nm, respectively, whereas A-A and Ni/A-A samples have broad pore-size distributions centred at 8.8 and 9.0 nm, respectively. The above findings are consistent with those obtained from TEM images.

TEM images of A-A and A-S supports are presented in Fig. 3. The A-A support has a nano-fibrous or lathlike morphology with non-uniform textural porosity [23,25], while the A-S support shows a typical wormhole-like morphology with a framework porosity [26,27]. It has been reported that the H_2O:Al precursor ratio determines the structure of CTAB-templated mesoporous alumina [22,23]. With increasing water content, the structure of the aluminas varies from a framework porosity to a textural porosity. In this work, however, mesoporous aluminas with different pore structures, i.e., framework porosity and textural porosity, can be synthesized even under the excess water condition. It is inferred that the identity of the basic solution dominantly governs the morphology of CTAB-templated mesoporous alumina, as demonstrated in Figs. 2 and 3. These results indicate that mesoporous γ-aluminas with different physical properties are successfully prepared via cationic surfactant-templating method by changing the identity of the basic solution.

Detailed physical properties of supports (A-A and A-S) and supported catalysts (Ni/A-A and Ni/A-S) are summarized in Table 1. Although the A-A support retains a lower surface-area, it has a larger pore volume and a larger average pore diameter than the A-S support. Both calcined Ni/A-A and Ni/A-S catalysts have a lower surface-area and a smaller pore volume than the corresponding support. This is due to pore blocking by the nickel species that occur during the impregnation step of the nickel precursor. On the other hand, both reduced Ni/A-A and Ni/A-S catalysts have almost the same physical properties as the calcined catalysts, and thereby indicate the high stability of the catalysts at high reduction temperatures.

Table 1
Physical properties of supports (A-A and A-S) and supported catalysts (Ni/A-A and Ni/A-S).

Sample	Surface-area ($cm^2\ g^{-1}$)[a]	Pore volume ($cm^3\ g^{-1}$)[b]	Average pore diameter (nm)[c]
A-A	162	0.47	8.8
Calcined Ni/A-A[d]	111	0.32	9.0
Reduced Ni/A-A[e]	104	0.34	9.6
A-S	271	0.35	3.5
Calcined Ni/A-S[d]	166	0.23	3.7
Reduced Ni/A-S[e]	168	0.26	4.2

[a] Calculated from the BET equation.
[b] BJH desorption pore volume.
[c] BJH desorption average pore diameter.
[d] Calcined at 700 °C for 5 h.
[e] Reduced at 700 °C for 3 h with mixed stream of H_2 and N_2.

3.2. Crystal structure of supports and supported catalysts

The XRD patterns of supports and supported catalysts are presented in Fig. 4. Both A-A and A-S supports show the characteristic diffraction peaks of γ-Al_2O_3 [28,29]. It is noticeable that the peaks corresponding to nickel oxide are not observed in both calcined Ni/A-A and Ni/A-S catalysts. This feature indicates that the nickel species are finely-dispersed on the surface of the Ni/A-A and Ni/A-S catalysts. It should be also noted that Ni^{2+} ions are incorporated into the lattice of γ-Al_2O_3, as demonstrated by the shift of the (4 4 0) diffraction peak of γ-Al_2O_3 [30-32]. This is further confirmed by calculating the lattice parameter of γ-Al_2O_3 in the supports and supported catalysts (Table 2). The lattice parameters of γ-Al_2O_3 in the A-A and A-S supports are 0.7877 and 0.7875 nm, respectively. After impregnating nickel on the support, however, the lattice parameters of γ-Al_2O_3 in the calcined Ni/A-A and Ni/A-S catalysts increase to 0.7968 and 0.7998 nm, respectively. Thus, the incorporation of Ni^{2+} into the lattice of γ-Al_2O_3 results in the lattice expansion of γ-Al_2O_3 [33,34]. This is due to the fact that the ionic

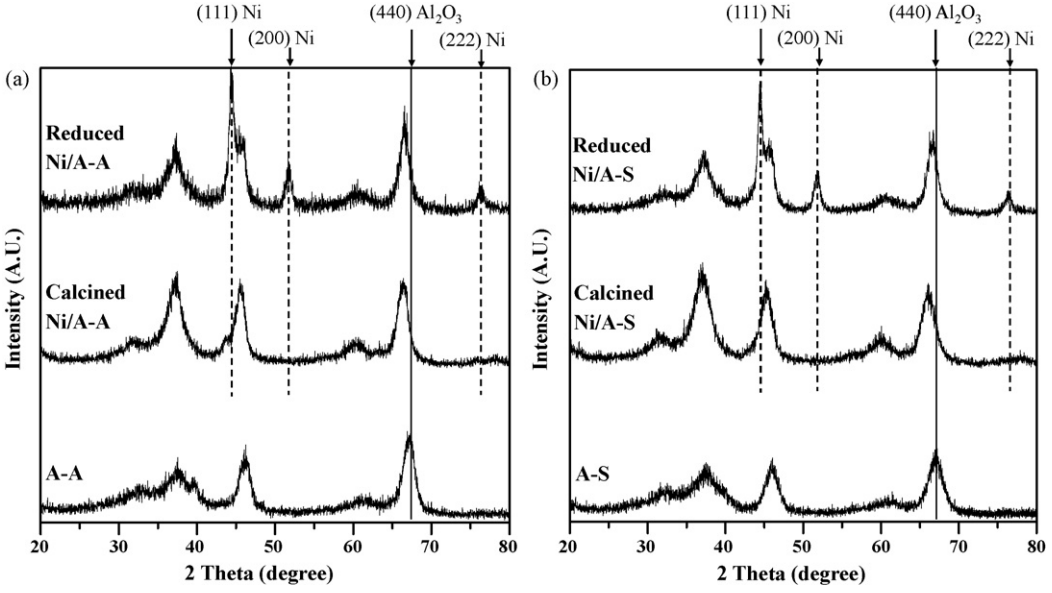

Fig. 4. XRD patterns of (a) A-A and Ni/A-A samples and (b) A-S and Ni/A-S samples. Supports and supported catalysts calcined at 700 °C. Supported catalysts reduced at 700 °C.

Table 2
Lattice parameter and nickel particle size.

Sample	Lattice parameter (nm)[a]	Ni particle size (nm)[b]
A-A	0.7877	–
Calcined Ni/A-A[c]	0.7968	n.d
Reduced Ni/A-A[d]	0.7951	21.8
A-S	0.7875	–
Calcined Ni/A-S[c]	0.7998	n.d
Reduced Ni/A-S[d]	0.7940	24.6

[a] Calculated from shift of Al_2O_3 (4 4 0) diffraction peak (Fig. 4).
[b] Calculated from Ni (2 2 2) diffraction peak broadening (Fig. 4).
[c] Calcined at 700 °C for 5 h.
[d] Reduced at 700 °C for 3 h with mixed stream of H_2 and N_2.

radius of Ni^{2+} is larger than that of Al^{3+}. Both reduced Ni/A-A and Ni/A-S catalysts exhibit diffraction peaks corresponding to metallic nickel (Fig. 4). As a consequence, the lattice parameters of γ-Al_2O_3 decreased from 0.7968 to 0.7951 nm for the reduced Ni/A-A catalyst and from 0.7998 to 0.7940 nm for the reduced Ni/A-S catalyst. The lattice parameter values of γ-Al_2O_3 in the reduced catalysts are not completely recovered to those of pure alumina supports, and this indicates the existence of a non-reducible nickel aluminate phase in the Ni/A-A and Ni/A-S catalysts. As also listed in Table 2, the particle size of nickel in the reduced Ni/A-A catalyst is a little smaller than that in the reduced Ni/A-S catalyst. In other words, the Ni/A-A catalyst exhibits relatively stronger metal–support interaction than the Ni/A-S catalyst.

3.3. Metal–support interaction

TPR measurements were carried out to investigate the reducibility of Ni/A-A and Ni/A-S catalysts and to examine the interaction between nickel species and supports. Fig. 5 (a) shows the TPR profiles of calcined Ni/A-A and Ni/A-S catalysts. Ni/A-A catalyst gives a narrow reduction band at around 835 °C, which might be due to the reduction of nickel aluminate phase [35,36]. This is well consistent with the XRD results (Fig. 4 and Table 2), showing the existence of nickel aluminate phase in the Ni/A-A catalyst. The Ni/A-S catalyst reports a major reduction band at around 810 °C with a shoulder at around 745 °C. This is due to the relatively high surface heterogeneity of the Ni/A-S catalyst compared to Ni/A-A catalyst. In other words, the Ni/A-S catalyst retains not only the nickel aluminate phase but also nickel oxide species. These observations indicate

Table 3
Degree of reduction and reduction peak temperature of reduced Ni/A-A and Ni/A-S catalysts.

Catalyst	Degree of reduction (%)[a]	Reduction peak temperature (°C)
Ni/A-A	95	795
Ni/A-S	98	834

[a] Degree of reduction (%) = [(area below H_2 consumption curve for calcined catalyst – area below H_2 consumption curve for reduced catalyst)/area below the H_2 consumption curve for calcined catalyst] ×100. Peak areas were calculated from Fig. 5.

that the interaction between the support and nickel species in the Ni/A-A catalyst is stronger than that in the Ni/A-S catalyst.

It is well known that the nickel aluminate phase is difficult to reduce because Ni^{2+} ions strongly interact with γ-Al_2O_3. This implies that nickel species in the calcined catalysts might not be fully reduced under the reduction condition. To calculate the degree of reduction of nickel species in the Ni/A-A and Ni/A-S catalysts, additional TPR measurements for the reduced catalysts have been conducted from room temperature to 930 °C. Prior to the TPR measurements, both Ni/A-A and Ni/A-S catalysts were reduced under the reduction condition employed in this work. Fig. 5 (b) shows the TPR profiles of reduced Ni/A-A and Ni/A-S catalysts. Both catalysts exhibit a small reduction peak corresponding to nickel aluminate species that are unreduced during the pre-reduction process. This is in good agreement with XRD results (Fig. 4). The degree of reduction and reduction peak temperature of the catalysts are summarized in Table 3. The degrees of reduction of Ni/A-A and Ni/A-S catalysts are 95% and 98%, respectively. Reduction peak temperature of each reduced catalyst (Fig. 5 (b)) is similar to that of the corresponding calcined catalyst (Fig. 5 (a)).

3.4. Steam reforming of LNG over Ni/A-A and Ni/A-S catalysts

Fig. 6 shows the LNG conversion and hydrogen composition in dry gas with time on stream in the steam reforming of LNG over Ni/A-C, Ni/A-A and Ni/A-S catalysts at 600 °C. The Ni/A-C catalyst experiences severe deactivation due to significant carbon deposition and the sintering of nickel species during the reaction, as reported in a previous work [16]. On the other hand, both Ni/A-A and Ni/A-S catalysts give relatively stable catalytic performance during reaction extending over 1000 min. The rea-

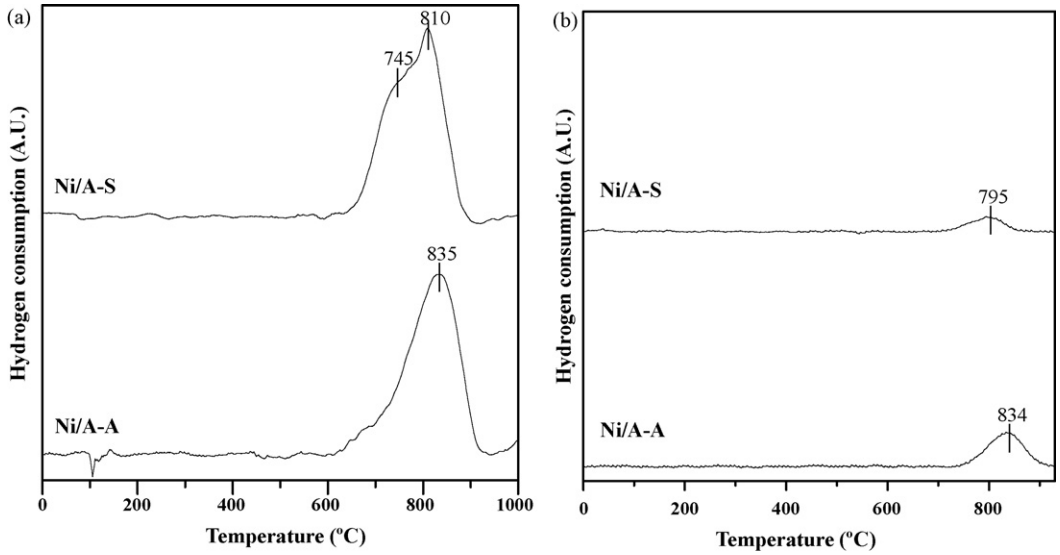

Fig. 5. TPR profiles of (a) calcined Ni/A-A and Ni/A-S catalysts and (b) reduced Ni/A-A and Ni/A-S catalysts.

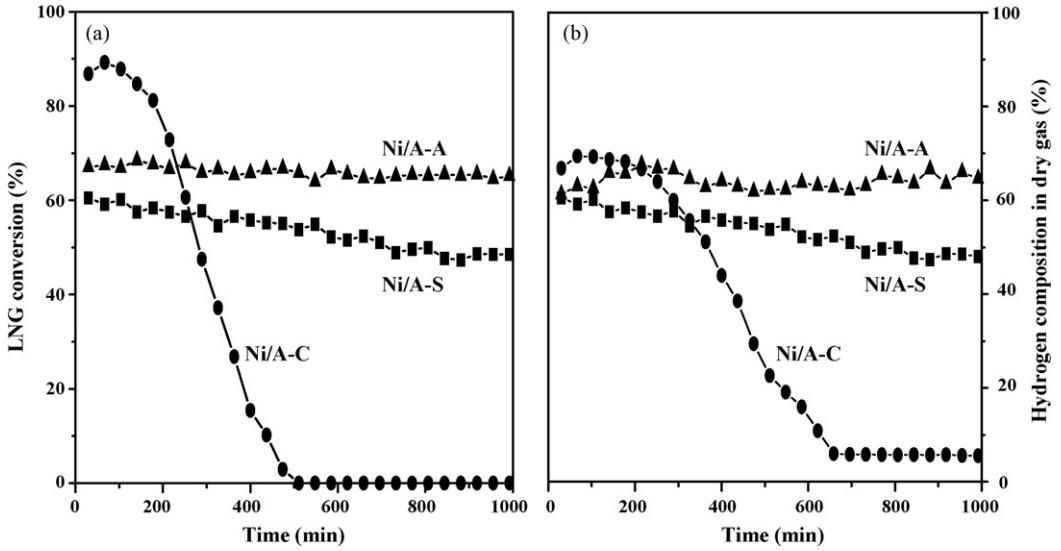

Fig. 6. (a) LNG conversions and (b) hydrogen composition in dry gas with time on stream in the steam reforming of LNG over Ni/A-C, Ni/A-A, and Ni/A-S catalysts at 600 °C.

sons why both Ni/A-A and Ni/A-S catalysts provide better catalytic performance than the Ni/A-C catalyst can be explained by their favourable physical and chemical properties. The high surface-area of A-A and A-S supports enhance the dispersion of nickel species, and results in a high active surface-area of metallic nickel in the Ni/A-A and Ni/A-S catalysts. The well-developed mesopores and strong metal–support interaction in the Ni/A-A and Ni/A-S catalysts effectively suppresss the sintering of nickel species and the carbon deposition during the steam reforming reaction. It is observed, however that the Ni/A-A catalyst exhibits a better catalytic performance than the Ni/A-S catalyst. This can be partly explained by the different pore structure between Ni/A-A and Ni/A-S catalysts. It is believed that the relatively large pore volume and large pore-size of Ni/A-A catalyst (Table 1) play an important role in facilitating internal mass transfer during the reaction.

The data in Fig. 6 also shows that the Ni/A-A catalyst has a stronger resistance towards catalyst deactivation than the Ni/A-S catalyst. This can be attributed to the different metal–support interaction between Ni/A-A and Ni/A-S catalysts. As shown by the TPR results (Fig. 5 (a)), the Ni/A-S catalyst retains relatively heterogeneous nickel oxide species compared with the Ni/A-A catalyst. It has been reported that reduced nickel aluminate has a higher intrinsic activity than the bulk metallic nickel in the reforming reaction [37]. Unlike the metallic nickel reduced from nickel oxide, moreover, metallic nickel reduced from nickel aluminate might be mono-dispersed on the catalyst surface, because the latter is closely associated with the alumina structure [37]. In other words, the reducible nickel aluminate in the Ni/A-A and Ni/A-S catalysts has high catalytic activity and strong resistance towards nickel sintering during the reforming reaction. On the other hand, nickel oxide species in the Ni/A-S catalyst can easily migrate and be aggregated

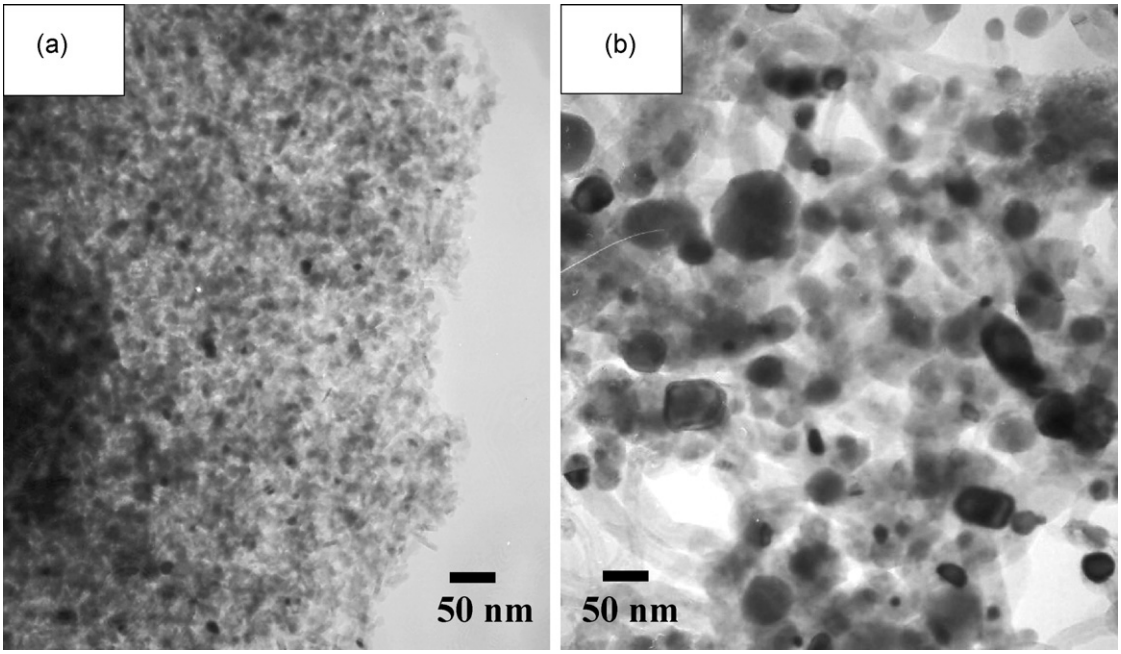

Fig. 7. TEM images of (a) Ni/A-A and (b) Ni/A-S catalysts after 1000 min reaction.

Table 4
Nickel particle size and carbon deposition in the used Ni/A-A and Ni/A-S catalysts.

Catalyst	Ni particle size (nm)[a]	Carbon deposition (wt%)[b]
Ni/A-A	22.9	0.9
Ni/A-S	38.8	3.1

[a] Calculated from Ni (2 2 2) diffraction peak broadening (not shown here).
[b] Obtained by CHNS elemental analyses.

at high reaction temperature. Therefore, the catalytic performance of Ni/A-S catalyst gradually decreases with time on stream. As listed in Table 4, it is revealed that the nickel particle size of the used Ni/A-S catalyst is about twice larger than that of the used Ni/A-A catalyst.

Fig. 7 shows TEM images of Ni/A-A and Ni/A-S catalysts after a 1000 min reaction. The used Ni/A-S catalyst contains filamentous carbon derived from the polymerization of dissolved carbon species on the active nickel surface. On the other hand, the used Ni/A-A catalyst showed no significant carbon deposition. CHNS elemental analyses reveal that the amount of carbon deposited on the Ni/A-S catalyst is much larger than that on the Ni/A-A catalyst (Table 4). In summery, the Ni/A-A catalyst has a strong resistance toward catalyst deactivation caused by carbon deposition and metal sintering.

4. Conclusions

Mesoporous γ-aluminas (A-A and A-S) have been prepared by a hydrothermal method under different basic conditions using cationic surfactant (CTAB) as a templating agent. Ni/γ-Al_2O_3 catalysts have been prepared by an impregnation method, and applied to hydrogen production by steam reforming of LNG. The effect of a mesoporous γ-Al_2O_3 support on the catalytic performance of Ni/γ-Al_2O_3 has been investigated. It is found that the identity of basic solution dominantly governs the physical properties of supports. The high surface-area of supports and the strong metal–support interaction of supported catalysts greatly enhance the dispersion of nickel species on the surface of Ni/A-A and Ni/A-S catalysts. The well-developed mesopores of Ni/A-A and Ni/A-S catalysts prohibit the polymerization of carbon species in the reaction. Both Ni/A-A and Ni/A-S catalysts give a better catalytic performance than the Ni/A-C catalyst in the steam reforming of LNG. Furthermore, the Ni/A-A catalyst shows a high and stable catalytic performance compared with the Ni/A-S catalyst. It has been found that relatively strong metal–support interaction of Ni/A-A catalyst suppresses sintering of metallic nickel as well as carbon deposition during the reaction. The large pore volume and large pore-size of the Ni/A-A catalyst are also favourable in facilitating internal mass transfer during the steam reforming reaction. Overall, it is concluded that the Ni/A-A serves as an efficient catalyst in hydrogen production by steam reforming of LNG.

Acknowledgements

The authors wish to acknowledge support from the Seoul Renewable Energy Research Consortium (Seoul R & BD Program) and RCECS (Research Center for Energy Conversion and Storage: R11-2002-102-00000-0).

References

[1] J.N. Armor, Appl. Catal. A 176 (1999) 159–176.
[2] K.D. Ko, J.K. Lee, D. Park, S.H. Shin, Korean J. Chem. Eng. 12 (1995) 478–480.
[3] J.G. Seo, M.H. Youn, S. Park, J. Lee, S.H. Lee, H. Lee, I.K. Song, Korean J. Chem. Eng. 25 (2008) 95–98.
[4] J.G. Seo, M.H. Youn, K.M. Cho, S. Park, S.H. Lee, J. Lee, I.K. Song, Korean J. Chem. Eng 25 (2008) 41–45.
[5] L. Kępiński, B. Stasińska, T. Borowiecke, Carbon 38 (2000) 1845–1856.
[6] T. Borowiecki, A. Gołębiowski, B. Stasińska, Appl. Catal. A 153 (1997) 141–156.
[7] O. Yokota, Y. Oku, T. Sano, N. Hasegawa, J. Matsunami, M. Tsuji, Y. Tamaura, Int. J. Hydro. Ener. 25 (2000) 81–86.
[8] K.O. Christensen, D. Chen, R. Lødeng, A. Holmen, Appl. Catal. A 314 (2006) 9–22.
[9] K. Kochloefl, in: G. Ertl, H. Knözinger, J. Weitkamp (Eds.), Handbook of Heterogeneous Catalysis, Vol.4, Wiley, New York, 1997, pp. 1819–1831.
[10] J. Čejka, Appl. Catal. A 254 (2003) 327–338.
[11] J. Čejka, N. Žilkova, L. Kaluža, Stud. Surf. Sci. Catal. 141 (2002) 243–250.
[12] M. Trueba, S.P. Trasatti, Eur. J. Inorg. Chem. 17 (2005) 3393–3403.
[13] T. Borowiecki, W. Gac, A. Denis, Appl. Catal. A 270 (2004) 27–36.
[14] J.S. Lisboa, D.C.R.M. Santos, F.B. Passos, F.B. Noronha, Catal. Today 101 (2005) 15–21.
[15] M.E.S. Hegarty, A.M. O'Connor, J.R.H. Ross, Catal. Today 42 (1998) 225–232.
[16] J.G. Seo, M.H. Youn, K.M. Cho, S. Park, I.K. Song, J. Power Sources 173 (2007) 943–949.
[17] J.-H. Kim, D.J. Suh, T.-J. Park, K.-L. Kim, Appl. Catal. A 197 (2000) 191–200.
[18] M. Yada, H. Hiyoshi, K. Ohe, M. Machida, T. Kijima, Inorg. Chem. 36 (1997) 5565–5569.
[19] J.C. Ray, K.-S. You, J.-W. Ahn, W.-S. Ahn, Micropor. Mesopor. Mater. 100 (2007) 183–190.
[20] S. Valange, J.-L. Guth, F. Kolenda, S. Lacombe, Z. Gabelica, Micropor. Mesopor. Mater. 35 (2006) 597–607.
[21] S.A. Bagshaw, T.J. Pinnavaia, Angew. Chem. Int. Ed. 35 (1996) 1102–1105.
[22] A. Beltrán, D. Beltrán, S. Mendioroz, M.D. Marcos, P. Amorós, Adv. Mater. 11 (1999) 379–381.
[23] H.C. Lee, H.J. Kim, C.H. Rhee, K.H. Lee, J.S. Lee, S.H. Chung, Micropor. Mesopor. Mater. 79 (2005) 61–68.
[24] J. Aguado, J.M. Escola, M.C. Castro, B. Paredes, Micropor. Mesopor. Mater. 83 (2005) 181–192.
[25] R.W. Hicks, N.B. Castagnola, Z. Zhang, T.J. Pinnavaia, C.L. Marshall, Appl. Catal. A 254 (2003) 311–317.
[26] W. Zhang, T.J. Pinnavaia, Chem. Commun. (1998) 1185–1186.
[27] P.T. Tanev, T.J. Pinnavaia, Science 267 (1995) 865–867.
[28] P. Kim, Y. Kim, H. Kim, I.K. Song, J. Yi, Appl. Catal. A 272 (2004) 157–166.
[29] X. Chen, K. Honda, Z. Zhang, Appl. Catal. A 279 (2005) 263–271.
[30] E.D. Dimotakis, T.J. Pinnavaia, Inorg. Chem. 29 (1990) 2393–2394.
[31] A. Corma, V. Fornes, R.M. Aranda, F. Rey, J. Catal. 134 (1992) 58–65.
[32] J.A. Wang, A. Morales, X. Bokhimi, O. Novaro, Chem. Mater. 11 (1999) 308–313.
[33] T. Ueckert, R. Lamber, N.I. Jaeger, U. Schubert, Appl. Catal. A 155 (1997) 75–85.
[34] G. Li, L. Hu, J.M. Hill, Appl. Catal. A 301 (2006) 16–24.
[35] J.G. Seo, M.H. Youn, I.K. Song, J. Mol. Catal. A 268 (2007) 9–14.
[36] Y. Zhang, G. Xiong, S. Sheng, W. Yang, Catal. Today 63 (2000) 517–522.
[37] J.R.H. Ross, M.C.F. Steel, A. Zeini-Isfahani, J. Catal. 52 (1978) 280–290.